Reductive TCA cycle enzymes and reductive amino acid synthesis pathways contribute to electron balance in a *Rhodospirillum rubrum* Calvin cycle mutant

Alexandra L. McCully[1,2†], Maureen C. Onyeziri[1†], Breah LaSarre[1], Jennifer R. Gliessman[1], and James B. McKinlay[1]*

[1]Department of Biology, Indiana University, Bloomington, IN

[2] Current address: Department of Civil and Environmental Engineering, Stanford University, CA

[†]Equal contributions.

*Corresponding author, jmckinla@indiana.edu

Keywords: electron balance, Calvin cycle, reductive tricarboxylic acid cycle, *Rhodospirillum rubrum, Rhodopseudomonas palustris*, purple nonsulfur bacteria

Abstract

Purple nonsulfur bacteria (PNSB) use light for energy and organic substrates for carbon and electrons when growing photoheterotrophically. This lifestyle generates more reduced electron carriers than are required for biosynthesis, even during consumption of some of the most oxidized organic substrates like malate and fumarate. Excess reduced electron carriers must be oxidized for photoheterotrophic growth to occur. Diverse PNSB commonly rely on the CO_2-fixing Calvin cycle to oxidize excess reduced electron carriers. Some PNSB also produce H_2 or reduce terminal electron acceptors as alternatives to the Calvin cycle. *Rhodospirillum rubrum* Calvin cycle mutants defy this trend by growing phototrophically on malate or fumarate without H_2 production or access to terminal electron acceptors. We used ^{13}C-tracer experiments to examine how a *Rs. rubrum* Calvin cycle mutant maintains electron balance under such conditions. We detected the reversal of some TCA cycle enzymes, which carried reductive flux from malate or fumarate to α-ketoglutarate. This pathway and the reductive synthesis of amino acids derived from α-ketoglutarate are likely important for electron balance, as supplementing the growth medium with α-ketoglutarate-derived amino acids prevented *Rs. rubrum* Calvin cycle mutant growth unless a terminal electron acceptor was provided. Flux estimates also suggested that the Calvin cycle mutant preferentially synthesized isoleucine using the reductive threonine-dependent pathway instead of the less-reductive citramalate-dependent pathway. Collectively, our results suggest that alternative biosynthetic pathways can contribute to electron balance within the constraints of a relatively constant biomass composition.

36 **Introduction**

37 Purple nonsulfur bacteria (PNSB) are a metabolically versatile group that are often
38 cultured under anaerobic conditions that support photoheterotrophic growth, wherein light is
39 used for energy and organic compounds are used for carbon and electrons. This lifestyle presents
40 a challenge in maintaining electron balance, as oxidative metabolic pathways generate an excess
41 of reduced electron carriers (i.e., reductant) (1, 2). Oxidation of excess reductant is essential for
42 growth and is often coupled to CO_2 fixation in the Calvin cycle. This is true even for growth on
43 substrates that are more oxidized than the average composition of cellular biomass, such as
44 acetate, succinate, malate, and fumarate (Table 1) (3). Calvin cycle mutants are generally
45 incapable of photoheterotrophic growth unless another means of electron disposal is possible,
46 such as the reduction of terminal electron acceptors, like dimethylsulfoxide (DMSO) (4-7), or H_2
47 production via nitrogenase (3, 8-11). Such trends have been observed for several PNSB
48 including *Rhodobacter sphaeroides* (4, 5, 7, 11), *Rhodobacter capsulatus* (6, 12), and
49 *Rhodopseudomonas palustris* (3, 8-10). An exception to this general observation is
50 *Rhodospirillum rubrum,* for which Calvin cycle mutants grow photoheterotrophically on malate
51 and fumarate without access to terminal electron acceptors and without producing H_2 (9, 13).
52 However, a terminal electron acceptor was still required by *Rs. rubrum* Calvin cycle mutants for
53 phototrophic growth on succinate, a more reduced substrate (Table 1) (9). The mechanism by
54 which *Rs. rubrum* Calvin cycle mutants maintain electron balance during phototrophic growth on
55 malate or fumarate is unknown, but the fact that growth only occurs on these relatively oxidized
56 substrates suggests that there is an inherent constraint on the amount of excess reducing
57 equivalents that can be dealt with.

58 Alternative central metabolic pathways that could maintain electron balance during
59 phototrophic growth in the absence of the Calvin cycle have been explored in silico (16), and
60 some have been ruled out. For example, phototrophic growth by Calvin cycle mutants on malate
61 could be possible if the cells produced formate (16). However, we previously found that *Rs.*
62 *rubrum* Calvin cycle mutants did not excrete formate, nor did they accumulate
63 polyhydroxybutyrate, an electron rich storage polymer that could potentially help maintain
64 electron balance (9). There is also evidence that an alternative CO_2-fixing pathway could be
65 involved, as an *Rs. rubrum* Calvin cycle mutant was observed to grow when CO_2 was the sole
66 carbon source (17). In *Rb. sphaeroides* and *Rs. rubrum*, the CO_2-fixing ethylmalonyl-CoA
67 pathway can substitute for the Calvin cycle to achieve electron balance during phototrophic
68 growth on acetate (18, 19). However, during phototrophic growth on malate, the ethylmalonyl-
69 CoA pathway is not expected to be active because malate is also the product of the pathway and
70 such a cycle would therefore be oxidative overall (16). Another CO_2-fixing mechanism that has
71 been proposed to participate in electron balance in *Rs. rubrum* Calvin cycle mutants is the partial
72 reversal of the TCA cycle, specifically, the reductive activity of α-ketoglutarate (αKG) synthase
73 that combines succinyl-CoA + CO_2 + reductant to form αKG (16, 20, 21).
74
75 Here we used ^{13}C-tracer experiments to gain insight into electron-balancing mechanisms
76 in a *Rs. rubrum* Calvin cycle mutant. Labeling patterns suggested net reductive TCA flux to αKG
77 from fumarate and malate. The reductive TCA cycle branch feeds into canonical reductive
78 pathways for the synthesis of αKG-derived amino acids. These amino acid synthesis pathways
79 likely also contribute to electron balance in a *Rs. rubrum* Calvin cycle mutant, as supplementing
80 the medium with αKG-derived amino acids prevented phototrophic growth on malate unless

81 DMSO was provided as a terminal electron acceptor. ^{13}C-tracer experiments using H_2-producing
82 strains of *Rp. palustris,* which requires the Calvin cycle or H_2 production to grow
83 phototrophically on malate or fumarate, suggest that both fumarate reductase and αKG synthase
84 are required for growth on malate or fumarate without the Calvin cycle. Flux estimates also
85 revealed the preferential use of the reductive threonine-dependent isoleucine synthesis pathway
86 over the less-reductive citramalate-dependent pathway in a *Rs. rubrum* Calvin cycle mutant but
87 not in *Rp. palustris*. Thus, *Rs. rubrum* appears to have flexibility within its biosynthetic pathways
88 that *Rp. palustris* does not, which can be used to satisfy electron balance during phototrophic
89 growth on substrates as oxidized as malate and fumarate.
90
91
92
93 **Results and Discussion**
94 **^{13}C-metabolic flux analysis of *Rs. rubrum* strains.** To gain insight into how *Rs. rubrum*
95 maintains electron balance without the Calvin cycle during phototrophic growth on relatively
96 oxidized substrates, we performed ^{13}C-metabolic flux analysis (^{13}C-MFA) to estimate in vivo
97 metabolic fluxes. In ^{13}C-MFA, the activities of different pathways generate signature patterns of
98 ^{12}C and ^{13}C that are imprinted on proteinaceous amino acids, which can be deciphered using gas
99 chromatography-mass spectrometry (GC-MS) (22). Software is then used to identify a set of
100 fluxes that can explain the observed mass isotopomer distributions (MIDs; i.e., labeling patterns).
101 Directly measured fluxes, such as those for excreted products and those needed to generate a
102 defined biomass composition, are also taken into account. We grew either wild-type (WT) *Rs.*
103 *rubrum* or a Calvin cycle mutant lacking genes for phosphoribulokinase (PRK) and ribulose-1,5-

104 bisphosphate carboxylase (RuBisCO), hereon referred to as the ΔPRKΔRubisco mutant (13), in a
105 defined medium with [1,4-^{13}C]fumarate. Cells harvested in exponential phase were used to
106 determine MIDs in proteinaceous amino acids. No H_2 was detected at the time of harvesting,
107 indicating that H_2 production was not involved in electron balance. High performance liquid
108 chromatography (HPLC) analysis of culture supernatants revealed that malate was excreted by
109 both strains, but more so by the ΔPRKΔRubisco mutant (46.2 ± 24.9 [± SD] mol malate/100 mol
110 fumarate] than the WT strain (8.5 ± 3.9 mol malate/100 mol fumarate). Malate excretion during
111 growth on fumarate has previously been observed in other bacteria, including *Rp. palustris* (3)
112 and *Geobacter sulfurreducens* (23). Malate accumulation could result from an imbalance
113 between the activities of fumarase and oxidative malate dehydrogenase when fumarate
114 concentrations exceed those normally encountered in nature. Alternatively, malate accumulation
115 might be necessary to make malate oxidation thermodynamically feasible (23). The higher level
116 of malate excretion in the ΔPRKΔRubisco mutant could be due to either, or both, a slower rate of
117 electron carrier oxidation that limits the NAD^+ available for malate oxidation or an accumulation
118 of NADH that increases the thermodynamic barrier for malate oxidation.
119
120 We then used the ^{13}C-MFA software INCA (24) to estimate a set of fluxes that could
121 explain the observed amino acid MIDs (Table S1), the malate excretion levels, and the *Rs.*
122 *rubrum* biomass composition (Table S2 and S3) using a redox-constrained model of *Rs. rubrum*
123 central metabolism and amino acid synthesis pathways (Table S4). For the biomass compositions
124 of the *Rs. rubrum* strains, we determined the protein content (75 ± 4% of the dry cell weight
125 [DCW]; statistically similar for both strains) and the amino acid composition (Table S3), and we
126 assumed that the remaining 25% of the DCW had a composition similar to that of *Rp. palustris*

127 (10). Our models originally included the ethylmalonyl-CoA pathway. Optimal solutions
128 indicated that a small reverse flux (<1% of the fumarate uptake rate) or exchange flux through
129 the ethylmalonyl-CoA pathway was needed to explain the level of m+2 glutamate (Glu) that we
130 observed. However, using INCAs simulation tool, we also found that exchange flux through only
131 one ethylmalonyl-CoA pathway reaction, namely, malate synthase, was sufficient to explain the
132 observed level of m+2 Glu (Fig. S1). We considered that exchange flux through malate synthase
133 was more likely than net flux in either direction through the entire 12-step pathway, which is
134 expected to be upregulated only during growth on C2 substrates like acetate (25), and as
135 described in the introduction, would not contribute to electron balance during growth on
136 compounds like malate or fumarate (16). The flux solutions we describe hereafter therefore
137 include reversible malate synthase but exclude the ethylmalonyl-CoA pathway. Optimal flux
138 solutions showed good agreement between the simulated and measured MIDs (Fig. S2). There
139 was also good agreement between most measured fluxes and simulated fluxes except for
140 summed biosynthetic redox reactions in the ΔPRKΔRubisco mutant and malate excretion for
141 both strains (Fig. S2). These few disagreements suggest that our flux solutions contain some
142 quantitative errors but, nevertheless, should point to qualitative trends that could contribute to
143 electron balance, which we address below.
144
145 ***Rs. rubrum* flux solutions suggest reductive flux from fumarate to αKG.** The flux maps for
146 both WT *Rs. rubrum* and the ΔPRKΔRubisco mutant revealed a bifurcation of the TCA cycle;
147 specifically, flux through an oxidative arm and flux through a reductive arm converged at αKG
148 (Fig. 1). Our flux estimates are consistent with the notion that *Rs. rubrum* lacks a complete
149 reverse TCA cycle but could still operate a reductive branch involving αKG synthase (20, 21).

150 Flux through αKG synthase was previously proposed as a mechanism by which a Calvin cycle
151 mutant could achieve electron balance (16, 21), based on αKG synthase activity detected in *Rs.*
152 *rubrum* cell extracts (20). We questioned whether the reductive flux from fumarate to αKG,
153 however small the estimated magnitude (0.1 and 0.6 mole % of the fumarate uptake rate in the
154 WT and ΔPRKΔRubisco strains, respectively), could be important for electron balance.
155
156 We first wanted to understand the labeling patterns that would be generated by reductive
157 flux from fumarate to αKG. Higher proportions of m+2 and m+3 Glu were observed in the
158 ΔPRKΔRubisco mutant compared to WT *Rs. rubrum* (Fig. 2). As noted above, malate synthase
159 exchange flux combined with either reductive or oxidative flux to αKG could generate m+2 Glu
160 (Fig. S1). From similar labeling experiments with *Rp. palustris*, we knew that m+3 metabolites,
161 including m+3 Glu, can be a signature of Calvin cycle activity during growth on substrates with
162 ^{13}C-labeled carboxyl groups (3). Without the Calvin cycle, we reasoned that m+3 Glu could be
163 generated from reductive flux from [1,4-^{13}C]fumarate to αKG when $^{13}CO_2$ is combined with
164 [1,4-^{13}C]succinyl-CoA to form [1,2,5-^{13}C]αKG, from which Glu is derived (Fig. 2A). The $^{13}CO_2$
165 needed for such a mechanism would come from the decarboxylation reactions stemming from
166 substrates with ^{13}C-labeled carboxyl groups (Fig. 2A) (3). Unlike m+3 Glu, other m+3 amino
167 acids were less abundant in the ΔPRKΔRubisco mutant than in the WT strain, which can also
168 generate m+3 metabolites via the Calvin cycle (Fig. 2A, Table S1). Thus, the mechanism by
169 which m+3 Glu was generated in the ΔPRKΔRubisco mutant must be within a few reactions
170 from Glu biosynthesis; reductive TCA flux from fumarate to αKG is consistent with such a
171 mechanism. Adjusting malate synthase activity using INCAs simulation tool indicated that

172 malate synthase cannot contribute to generating m+3 Glu, suggesting that reductive αKG
173 synthase is solely responsible for generating m+3 Glu in the ΔPRKΔRubisco mutant.
174
175 INCA's simulation tool does not produce a new optimal solution every time an individual
176 flux is adjusted. Thus, to confirm that reductive flux to αKG was the only mechanism that could
177 generate m+3 Glu in the ΔPRKΔRubisco mutant, we ran fitting algorithms using a model in
178 which αKG synthase flux was constrained to be strictly forward (i.e., oxidative). Whereas
179 optimal solutions for WT *Rs. rubrum* models with strictly oxidative αKG synthase activity could
180 fully explain the Glu labeling patterns, optimal solutions for the ΔPRKΔRubisco mutant resulted
181 in a disagreement between the simulated and observed levels of m+3 Glu (Fig. 2B, C). In fact,
182 without the Calvin cycle or reductive αKG synthase flux, the optimal solutions could not
183 generate m+3 Glu (Fig. 2B, C). Thus, reductive flux to αKG is the only mechanism that can
184 generate m+3 Glu in the ΔPRKΔRubisco mutant.
185 MIDs from a separate labeling experiment, wherein *Rs. rubrum* strains were cultured
186 with unlabeled malate and $NaH^{13}CO_3$ as a source of $^{13}CO_2$, also suggested net reductive flux to
187 αKG for both WT and ΔPRKΔRubisco mutant strains (0.7 and 4.6 mole % of the fumarate
188 uptake rate, respectively), in this case from malate (Fig. 3, yellow inset; Table S4). We expected
189 that providing $NaH^{13}CO_3$ would result in the labeling of Glu by the reductive carboxylation of
190 succinyl-CoA to αKG. However, both Glu and all other amino acids analyzed showed
191 enrichment of m+1 isotopomers to varying degrees (Fig. 3; Table S1), which likely resulted from
192 carboxylation via the Calvin cycle (WT strain only) and exchange flux through carboxylation
193 reactions (both strains), such as those between PEP and oxaloacetate, between pyruvate and
194 acetyl-CoA, and those in the citramalate-dependent isoleucine biosynthesis pathway; these

195 possibilities were verified using INCAs simulation tool. Importantly, these reactions alone could
196 not fully explain the measured Glu MIDs. In both strains, although only approximately 20% of
197 aspartate, derived from oxaloacetate, had a mass of m+1, more than 30% of Glu, derived from
198 αKG, had a mass of m+1 Glu. (Fig. 3). Thus, some of the m+1 Glu must have been derived from
199 reductive flux from unlabeled malate to αKG. The ΔPRKΔRubisco mutant also exhibited a
200 higher proportion of m+2 and m+3 Glu isotopomers compared to the WT strain (Fig. 3). These
201 higher molecular weight Glu isotopomers could only be explained by the reductive carboxylation
202 of single- and double-labeled succinyl-CoA, which itself must have been derived from exchange
203 flux from single- and double-labeled oxaloacetate (Fig. 3). Both INCA simulations and
204 sensitivity matrixes indicated that Glu labeling was relatively insensitive to malate synthase
205 exchange flux under these experimental conditions, thus malate synthase was not a source of
206 these labeling patterns. Thus, the results of two separate labeling experiments indicated reductive
207 flux to αKG through multiple reactions typically associated with the reductive TCA cycle as a
208 compensatory response to the absence of the Calvin cycle in the *Rs. rubrum* ΔPRKΔRubisco
209 mutant.
210
211 **αKG-derived amino acids inhibit growth of the *Rs. rubrum* ΔPRKΔRubisco mutant.** Similar
212 to our findings with photoheterotrophic *Rp. palustris* (3, 10), the relatively small flux to αKG in
213 our *Rs. rubrum* flux maps was primarily dictated by the need for αKG as a biosynthetic
214 precursor; although reductive to flux to αKG might play a role in electron balance, the flux did
215 not exceed that needed to synthesize the amino acids Glu, Gln, Pro, and Arg. These four amino
216 acids are all produced via reductive pathways and thus could also contribute to electron balance
217 (Fig. 1C and 4A). In other bacteria, such as *E. coli*, the presence of each of these amino acids

218 inhibits its own synthesis (26-30). We predicted that if these amino acid synthesis pathways are
219 similarly regulated in *Rs. rubrum*, then their synthesis could be repressed by including them in
220 the growth medium; in this manner, supplementation with these amino acids might prevent
221 reductive flux to αKG. Addition of the four amino acids (EQPR) had no effect on the
222 phototrophic growth trends of WT *Rs. rubrum* grown on malate but prevented ΔPRKΔRubisco
223 mutant growth (Fig. 4B). These results could be interpreted to mean that adding Glu, Gln, Pro,
224 and Arg inhibited the respective amino acid synthesis pathways and thereby prevented electron
225 balance. An alternative explanation could be that, even at 0.2 mM each, the catabolism of these
226 amino acids contributed to an excess of reductant. However, adding four amino acids derived
227 from oxaloacetate (DTMK) did not affect growth of either WT or the ΔPRKΔRubisco mutant on
228 malate (Fig. 4C). The addition of either 0.7 mM isoleucine (Fig. 5) or 0.7 mM leucine (data not
229 shown), both of which should also generate reductant through their catabolism, also did not
230 affect the growth of the ΔPRKΔRubisco mutant on malate. Thus, the inhibitory effect of Glu,
231 Gln, Pro, and Arg on the ΔPRKΔRubisco mutant is specific to this amino acid mixture. To verify
232 that the growth inhibition was linked to electron balance rather than to an unrelated form of
233 toxicity, we repeated the growth experiment in medium supplemented with the terminal electron
234 acceptor DMSO. Adding DMSO rescued ΔPRKΔRubisco mutant growth on malate in the
235 presence of Glu, Gln, Pro, and Arg (Fig. 4D). Thus, the addition of Glu, Gln, Pro, and Arg
236 created a growth-inhibiting electron imbalance in the ΔPRKΔRubisco mutant.
237
238 Our attempts to genetically determine whether reductive flux to αKG was essential were
239 inconclusive. *Rs. rubrum* is annotated to have both irreversible αKG dehydrogenase
240 (Rru_A1213–A1215) and reversible αKG synthase (Rru_A2720–A2722). We deleted

241 Rru_A2721, annotated to encode the αKG synthase α-subunit, in a ΔPRK mutant (UR2565) (13).
242 The ΔPRK strain cannot fix CO_2 via the Calvin cycle, has similar growth trends to the
243 ΔPRKΔRubisco mutant (9), and has the genetic background necessary for genetic engineering
244 (unlike the ΔPRKΔRubisco mutant, the ΔPRK strain is not resistant to gentamycin, which is
245 needed to select for integration of the suicide vector). Unfortunately, the ΔPRKΔRru_A2721
246 mutant exhibited a high incidence of H_2 production (10 of 12 biological replicates across four
247 independent experiments grew accompanied by H_2 production), likely due to a spontaneous
248 mutation that activates nitrogenase; such suppressor mutations are known to improve the growth
249 of *Rs. rubrum* Calvin cycle mutants (31). The production of H_2 could suggest that H_2 production
250 was necessary for the mutant to grow. However, the high frequency of H_2 production prevented
251 us from making a definitive conclusion about the essentiality of αKG synthase in the absence of
252 the Calvin cycle.
253
254 **Isoleucine is produced primarily by a reductive pathway in the *Rs. rubrum* ΔPRKΔRubisco**
255 **mutant.** *Rs. rubrum* has two pathways for isoleucine synthesis. The canonical threonine-
256 dependent pathway uses 1 oxaloacetate and 1 pyruvate, whereas the alternative citramalate-
257 dependent pathway uses 1 AcCoA and 2 pyruvate (Fig. 5A) (32). Although both pathways are
258 technically reductive, we herein consider the citramalate-dependent pathway to be oxidative
259 because the path from fumarate or malate to 2 pyruvate + 1 AcCoA generates more reducing
260 equivalents than can be oxidized in the subsequent synthesis of isoleucine (Fig. 5A). The optimal
261 flux solutions for *Rs. rubrum* strains grown on [1,4-^{13}C]fumarate estimated that the WT strain
262 used the threonine-dependent pathway to make 76% of the isoleucine, whereas the
263 ΔPRKΔRubisco mutant used this pathway to make 85% of the isoleucine (Fig. 5B). Flux
264 solutions from conditions using unlabeled malate and $Na^{13}CO_3$ were more skewed, indicating

265 that isoleucine was made primarily by the oxidative citramalate-dependent pathway in the WT
266 strain, whereas the reductive threonine-dependent pathway was dominant in the ΔPRKΔRubisco
267 mutant (Fig. 5B). Overall, the ^{13}C-MFA solutions suggest that the threonine-dependent
268 isoleucine synthesis pathway is used as a compensatory mechanism for maintaining electron
269 balance in the absence of the Calvin cycle. The flexibility that the two isoleucine synthesis
270 pathways impart in the management of electrons could explain why both seemingly redundant
271 pathways are maintained in some bacteria (32-34).
272
273 To assess whether the reductive isoleucine pathway was essential for electron balance in
274 the absence of the Calvin cycle, we deleted *ilvA* (Rru_A2877), encoding threonine dehydratase,
275 in both WT *Rs. rubrum* and the ΔPRK mutant to prevent isoleucine synthesis via the threonine-
276 dependent pathway. Separately, we also grew WT and ΔPRKΔRubisco *Rs. rubrum* strains in the
277 presence of isoleucine, which has the potential to inhibit both isoleucine synthesis pathways if
278 the pathways are regulated in *Rs. rubrum* as they are in *E. coli* (35) and *Leptospira interrogans*
279 (36). Neither deleting *ilvA* (Fig. 5C) nor adding isoleucine to the growth medium (Fig. 5D)
280 affected the growth trends of either the WT or the Calvin cycle mutants. No H_2 accumulated
281 during the course of these experiments. Thus, although the ^{13}C labeling patterns suggested that
282 the flux through the two isoleucine synthesis pathways was influenced by the need to maintain
283 electron balance, the reductive threonine-dependent pathway is not essential for electron balance
284 in *Rs. rubrum* Calvin cycle mutants.
285
286 **Sulfide production does not participate in electron balance in *Rs. rubrum*.** Reduction of
287 sulfate to sulfide by a spontaneous mutant of *Rb. sphaeroides* was previously implicated as an

288 alternative electron-balancing mechanism during photoheterotrophic growth (37). Thus, we also
289 considered whether sulfate reduction could contribute to electron balance in *Rs. rubrum*.
290 However, using lead acetate strips, we did not detect any sulfide in either WT or ΔPRKΔRubisco
291 mutant cultures (Fig. S3).
292
293 **Why is the Calvin cycle required by *Rp. palustris* for photoheterotrophic growth?** *Rs.*
294 *rubrum* Calvin cycle mutants can grow on fumarate and malate, whereas *Rp. palustris* Calvin
295 cycle mutants cannot unless they can dispose of excess electrons as H_2 (9). The *R. palustris*
296 CGA009 genome is annotated to have an α-oxoacid ferredoxin oxidoreductase (RPA1225–
297 1228), suggesting that it could be capable of reductive αKG synthase activity. We considered
298 that the reason *Rp. palustris* Calvin cycle mutants cannot grow on malate or fumarate might be
299 due to an inability to reduce fumarate, which would deny αKG synthase from participating in
300 electron balance during growth on fumarate and malate. All *Rp. palustris* strains tested by other
301 groups have not exhibited fumarate reductase activity, unlike *Rs. rubrum* (38, 39). In *Rs. rubrum*,
302 fumarate reductase activity is dependent on rhodoquinone (38), a compound that is notably
303 absent from all *Rp. palustris* strains that have been analyzed (38, 40-42). Our BLAST searches
304 against the *R. palustris* CGA009 genome (43) using the only known *Rs. rubrum* protein required
305 for rhodoquinone synthesis, namely, the methyltransferase RquA, (Rru_A3227) (44), also
306 suggested that *Rp. palustris* cannot synthesize rhodoquinone; the top hit was RPA0138,
307 annotated as the chemotaxis methyl transferase CheR1, with only 31% coverage and 28% amino
308 acid identity (E value: 0.002).
309

310 To assess whether *R. palustris* is capable of fumarate reductase and reductive αKG
311 synthase activities in vivo, we performed four separate labeling experiments with an H_2-
312 producing *Rp. palustris* NifA* strain, CGA676, and its ΔPRKΔRubisco mutant counterpart,
313 CGA4011 (9), and either [1,4-^{13}C]succinate, [1,4-^{13}C]fumarate, unlabeled succinate with
314 $NaH^{13}CO_3$, or unlabeled malate with $NaH^{13}CO_3$. We used two models for each strain: one that
315 allowed for reversible αKG synthase activity, and another that allowed for only oxidative αKG
316 synthase activity. If *Rp. palustris* carried out reversible αKG synthase activity under these
317 growth conditions then we expected that reductive αKG synthase activity would be required to
318 explain Glu labeling patterns in the NifA* ΔPRKΔRubisco mutant during growth on succinate.
319 If *Rp. palustris* is incapable of fumarate reductase activity then we expected that reductive αKG
320 synthase activity would not be required to explain Glu labeling patterns on fumarate or malate, as
321 there would be no way to reduce either of these compounds to the succinyl-CoA needed for
322 reductive αKG synthase activity.
323 In models that allowed for reversible of αKG synthase activity, the optimal solutions
324 showed net reductive flux to αKG when the NifA*ΔPRKΔRubisco mutant was grown with either
325 [1,4-^{13}C]succinate or succinate with $NaH^{13}CO_3$ (Fig. 6A). Net oxidative αKG synthase flux was
326 estimated in all *Rp. palustris* NifA* conditions and in NifA*ΔPRKΔRubisco mutant conditions
327 supplied with either [1,4-^{13}C]fumarate or malate with $NaH^{13}CO_3$ (Fig. 6A). These solutions
328 support the notion that *Rp. palustris* is capable of reductive αKG synthase activity but not
329 fumarate reductase activity. The estimated reductive αKG synthase flux in the
330 NifA*ΔPRKΔRubisco strain only could suggest that reductive αKG synthase activity provided
331 some compensatory electron-balancing activity during growth on succinate in the absence of the
332 Calvin cycle, despite being unessential given the requirement for H_2 production (3, 10).

333 However, it is noteworthy that markedly less m+3 Glu was generated by *Rp. palustris* NifA*
334 ΔPRKΔRubisco compared to *Rp. palustris* NifA* during growth on [1,4-^{13}C]succinate (Fig. 6B).
335 Similarly, the abundance of m+1, m+2, and m+3 Glu was less in *Rp. palustris* NifA*
336 ΔPRKΔRubisco compared to *Rp. palustris* NifA* when grown with succinate with $NaH^{13}CO_3$.
337 These observations are opposite of the trends observed with *Rs. rubrum* and thus strongly
338 suggest that reductive flux to αKG is not a general mechanism used by *Rp. palustris* in response
339 to the loss of the Calvin cycle, at least during phototrophic growth on succinate when H_2 is
340 produced.
341
342 When the models were constrained to allow for only oxidative αKG synthase activity,
343 Glu MIDs could still be explained for both *Rp. palustris* strains under most conditions.
344 Experiments with $NaH^{13}CO_3$ did not determine αKG synthase activity with confidence in the
345 NifA* ΔPRKΔRubisco mutant (Fig. 6A). However, similar to our observations with *Rs. rubrum*,
346 reductive αKG synthase activity was required to generate m+3 Glu in the model for the NifA*
347 ΔPRKΔRubisco mutant grown on [1,4-^{13}C]succinate (Fig. 6C). The fact that reductive αKG
348 synthase activity was required in this case but was not required to explain Glu labeling patterns
349 when the NifA* ΔPRKΔRubisco mutant was grown on [1,4-^{13}C]fumarate (Fig. 6C; data for other
350 conditions not shown) supports the notion that there is no fumarate reductase activity to supply
351 double-labeled succinate from which m+3 Glu would ultimately be derived (Fig. 2A). Thus,
352 overall, there is good evidence that the inability to reduce fumarate is the reason why *Rp.*
353 *palustris* Calvin cycle mutants cannot grow phototrophically on malate or fumarate without
354 producing H_2.
355

356 Although not expected to be an essential electron-balancing mechanism based on our data
357 with *Rs. rubrum* (Fig. 8), we also examined whether H_2-producing *Rp. palustris* adjusted fluxes
358 through the same two isoleucine synthesis pathways (3, 10) in response to the loss of the Calvin
359 cycle. Unlike for *Rs. rubrum*, the oxidative citramalate-dependent pathway was estimated to
360 dominate under all but one condition, and flux through the reductive threonine-dependent
361 pathway did not increase in response to the absence of the Calvin cycle (Fig. S4).
362
363 **Conclusion.** Our data support previous results from our own group (9) and others (13) that *Rs.*
364 *rubrum* can maintain electron balance during photoheterotrophic growth on malate and fumarate
365 without the Calvin cycle, H_2 production, or access to terminal electron acceptors. Our results
366 suggest that a *Rs. rubrum* Calvin cycle mutant can maintain electron balance during phototrophic
367 growth on malate and fumarate by selectively utilizing various biosynthetic pathways. The
368 relatively static nature of biomass composition for a given growth condition places constraints on
369 the extent to which different biosynthetic pathways can be employed to achieve electron balance
370 and thus likely explains why a *Rs. rubrum* Calvin cycle mutant cannot grow with succinate,
371 which has only two more electrons than malate or fumarate (Table 1). The two biosynthetic
372 pathways we identified to contribute to electron balance in *Rs. rubrum* were (i) reductive flux
373 from fumarate to αKG linked to the reductive synthesis of amino acids from αKG and (ii) the
374 preferential use of the reductive threonine-dependent pathway for isoleucine synthesis instead of
375 the less-reductive citramalate-dependent pathway. Given the relatively minor influence the
376 pathways are estimated to have on electron balance (Fig. 1C), it is possible that other
377 biosynthetic pathways not be detected by our approach, such as altered fatty acid composition,
378 could also offer limited flexibility to contribute to electron balance. Flexibility in electron

379 management could explain why some bacteria maintain seemingly redundant biosynthetic
380 pathways, such as those for isoleucine synthesis and those supplying αKG for amino acid
381 synthesis. Our flux estimates suggest that αKG can be synthesized by via both reduction and
382 oxidation of TCA cycle intermediates from malate and fumarate in *Rs. rubrum* and from
383 succinate in *Rp. palustris*. Such activities would add these two PNSB to a short list of bacteria
384 known to produce αKG-derived amino acids via two separate pathways (45, 46). The previous
385 detection of fumarate reductase activity in diverse PNSB (38, 39) raises the possibility that such
386 dual pathways might be found in other PNSB as well and perhaps play a conserved role in
387 electron balance during photoheterotrophic growth in these bacteria.
388
389 **Methods.**
390 **Strains and growth conditions.** *Rs. rubrum* strains ΔPRKΔRubisco (UR2557, Δ*cbbM::*Gm^R
391 Δ*cbbP*::Km^R (13)) and ΔPRK (UR2565, Δ*cbbP*::Km^R (13)) were derived from type-strain UR2
392 (47). *Rp. palustris* strains CGA676 (NifA*, (10)) and CGA4011 (NifA*, Δ*cbbLS*, Δ*cbbM*,
393 Δ*cbbP*::Km^R (9)) were derived from type-strain CGA009. *Rs. rubrum* or *Rp. palustris* strains
394 were revived from frozen stocks containing 10% DMSO or 25% glycerol, respectively, by
395 streaking for single colonies on defined photosynthetic medium (PM) agar (48) supplemented
396 with 10 mM disodium succinate and 0.1% yeast extract without antibiotics. Colonies were then
397 used to inoculate 3 ml aerobic starter cultures of PM (*Rp. palustris*) or defined MA medium (*Rs.*
398 *rubrum*) (9), each with 10 mM succinate. Aerobic starter cultures were grown at 30°C with
399 shaking at 150 rpm. A 0.1-ml inoculum from stationary phase aerobic starter cultures was then
400 transferred into 10 ml of anaerobic PM (*Rp. palustris*) or MA (*Rs. rubrum*) supplemented with
401 10 mM of an organic substrate, as indicated, in 28-ml anaerobic test tubes sealed with rubber
402 stoppers under an argon headspace, as described (9). Where indicated, media were supplemented

403 with specific amino acids (20 mg/L each), DMSO (60mM), or $NaHCO_3$ (20 mM), prior to
404 inoculation. Antibiotics were not used in comparative growth experiments or in ^{13}C-labeling
405 experiments but were otherwise added to media where appropriate. Gentamycin and kanamycin
406 were each used at 100 µg/ml for *Rp. palustris* and at 10 µg/ml for *Rs. rubrum*. *Bacillus subtilis*
407 3610 (49) and *Escherichia coli* strains NEB10β (New England Biolabs) and WM3064 were
408 cultured aerobically on LB agar or in LB broth. WM3064 is a diaminopimelic acid (DAP)
409 auxotroph and was thus supplemented with 0.6 mM DAP (W. Metcalf, unpublished data).
410 Gentamycin was used at 15 µg/ml for *E. coli*.
411 **Analytical techniques.** Cell density was assayed by optical density (OD_{660}) using a Genesys 20
412 visible spectrophotometer (Thermo-Fisher, Pittsburgh, PA). Specific growth rates were
413 determined using measurements with values between 0.1 – 0.8 OD_{660}, where a linear relationship
414 between cell density and OD_{660} was maintained. H_2 was sampled from culture headspace using a
415 gas-tight syringe and analyzed using a Shimadzu GC-2014 gas chromatograph as described (50).
416 Organic acid levels in culture supernatants were determined by HPLC (Shimadzu) as described
417 (51). Sulfide was detected using lead acetate strips suspended above the cultures. Strips were
418 removed and photographed once cultures reached stationary phase (52).
419 ***Rs. rubrum* biomass composition.** Measurements were performed for the WT strain (UR2) and
420 the ΔPRKΔRubisco mutant (UR2557) grown in MA medium. Culture samples were taken
421 between 0.08 and 0.85 OD_{660} as measured using plastic cuvettes with a 1-cm path length. DCWs
422 were determined as described (53) by filtering 30-mL of culture through preweighed 0.22-µm
423 HA filters (Millipore) and then drying the filters overnight at 80 °C. Protein was quantified using
424 a bicinchoninic acid assay (Pierce) as described (10). Amino acid composition was determined
425 using a Hitachi L-8800 amino acid analyzer at the University of California, Davis Molecular

426 Structure Facility. The polyhydroxybutyrate content was previously found to be below the
427 detection limit (9). Because protein accounted for 75% of the DCW, the remaining DCW not
428 accounted for in protein was assumed to comprise other major macromolecules at the same
429 proportions as found in *Rp. palustris* and with the same monomeric composition. A common
430 biomass composition was used for both strains because the slopes for linear regression of
431 DCW/L vs. OD_{660} (400 ± 40 mg/L/ OD_{660}) and protein vs. DCW (75 ± 4% of DCW) were
432 statistically similar ($p > 0.1$, determined using the linear regression analysis function in
433 Graphpad Prism 6.0).
434 **^{13}C-labeling experiments and metabolic flux analysis.** Three or four biological replicates of
435 each strain were inoculated from unlabeled starter cultures into media containing the indicated
436 ^{13}C-labeled substrate, provided at 100%. Cultures were harvested in exponential phase between
437 0.2 – 0.7 OD_{660} as described previously (10). Amino acids were obtained from the cell pellets by
438 hydrolysis in 6 N HCl, the amino acids were derivatized, and then MIDs were determined using
439 GC-MS as described (53) at the Indiana University Mass Spectrometry Facility. MIDs were
440 corrected for natural abundances of all atoms except for carbons in amino acid backbones using
441 the IsoCor software (54). Corrected amino acid MIDs and flux measurements (i.e., excreted
442 malate or fumarate and fluxes derived from the biomass composition [Table S2]) were used with
443 a metabolic model and the software INCA (24) to map the carbon atom transitions through the
444 central metabolism of *Rs. rubrum* or *Rp. palustris* (Table S4). Our *Rs. rubrum* model included
445 the TCA cycle, gluconeogenesis/glycolysis, the Calvin cycle, the pentose phosphate pathway,
446 and the ethylmalonyl-CoA pathway (Table S4). Models that required that the sum of fluxes
447 through reduction reactions equal the sum of fluxes through oxidation reactions included terms
448 representing oxidized electron carriers (X) and reduced electron carriers (XH) in each redox

449 reaction. Equations were also included to reflect the reductant required for biosynthesis and the
450 reductant generated by biosynthesis. For each condition or model variation tested, at least 100
451 different arrangements of starting free parameter values were used. An optimal solution was
452 selected based on that which had the lowest sum of squared residuals between the simulated and
453 measured data sets for MIDs and biosynthetic and extracellular fluxes. Upper and lower bounds
454 for flux values were determined using INCAs parameter continuation tool.
455 ***Rs. rubrum* strain construction.** To create an in-frame deletion of Rru_A2721 (αKG synthase
456 α-subunit), the region upstream of Rru_A2721 was amplified using primers BL501
457 (gacttctagactataacgatctggccgattggc) and BL524 (gactggtacccgtcatcatccgtctttcagagaag), and the
458 region downstream was amplified using primers BL525 (gactggtacccagggagagtgatcatggatacg)
459 and BL504 (gacttctagaactgggcttcgatttcggtgaa). The resulting PCR products were digested using
460 KpnI and ligated together, and then the ligation reaction was used as template for a second round
461 of PCR using primers BL501 and BL504. The resulting PCR product was purified, digested with
462 XbaI, and then ligated into XbaI-digested pJQ200SK (55). To create an in-frame deletion of
463 Rru_A2877 (*ilvA*, threonine deaminase), the upstream region was amplified using primers
464 BL646 (gctggagctccaccgtgactccgtctggccccaag) and BL635 (tccccggcggtcatcgtccgccctcc), and the
465 downstream region was amplified using primers BL636 (cgatgaccgccggggattagggcaaatc) and
466 BL647 (attcctgcagcccggcgtcgattacaccggcctc). The upstream and downstream PCR products were
467 mixed with pJQ200SK, which was PCR-linearized using primers BL644 (cggtggagctccagcttttg)
468 and BL645 (ccgggctgcaggaattcg), and then assembled by Gibson Assembly (NEB). Ligation and
469 Gibson reactions were transformed into *E. coli* NEB10β (New England Biolabs), and
470 transformants were verified by PCR and sequencing. Vectors were first introduced into
471 electrocompetent *E. coli* WM3064 and were then transferred to *Rs. rubrum* strains by

472 conjugation on PM agar with yeast extract, succinate, and DAP. Mating patches were streaked
473 for single recombinants on PM agar with yeast extract, succinate, and Gm (no DAP). Colonies
474 were then grown in liquid medium without Gm to allow for a second recombination event.
475 Cultures were plated on PM agar with yeast extract, succinate, and 10% sucrose, resultant
476 colonies were screened for Gm sensitivity, and then Gm-sensitive colonies were screened by
477 PCR for the desired deletions.
478
479 **Author statements.**
480 JBM conceived the study. All authors performed experiments. ALM, MCO, JRG, and JBM
481 analyzed the data. JBM wrote the initial manuscript draft. ALM, BL, and JBM edited subsequent
482 drafts. All authors reviewed and approved the final draft.
483
484 The authors declare no conflict of interest.
485
486 This work was funded by the Indiana University College of Arts and Sciences.
487
488 We thank GC Gordon for contributions to preliminary studies, JA Karty for GC-MS training and
489 advice, and anonymous reviewers for insightful questions that led to the improvement of this
490 work.
491
492 **References**

493 1. **Erb TJ**. Carboxylases in natural and synthetic microbial pathways. *Appl Environ*
494 *Microbiol.* 2011;77:8466-77.
495 2. **Muller FM**. On the metabolism of the purple sulphur bacteria in orgainic media. *Arch*
496 *Microbiol.* 1933;4:131-66.

497 3. **McKinlay JB, Harwood CS**. Calvin cycle flux, pathway constraints, and substrate
498 oxidation state together determine the H_2 biofuel yield in photoheterotrophic bacteria.
499 *mBio*. 2011;2:e00323-10.
500 4. **Hallenbeck PL, Lerchen R, Hessler P, Kaplan S**. Roles of CfxA, CfxB, and external
501 electron acceptors in regulation of ribulose 1,5-bisphosphate carboxylase/oxygenase
502 expression in *Rhodobacter sphaeroides*. *J Bacteriol*. 1990;172:1736-48.
503 5. **Hallenbeck PL, Lerchen R, Hessler P, Kaplan S**. Phosphoribulokinase activity and
504 regulation of CO_2 fixation critical for photosynthetic growth of *Rhodobacter sphaeroides.*
505 *J Bacteriol*. 1990;172:1749-61.
506 6. **Paoli GC, Vichivanives P, Tabita FR**. Physiological control and regulation of the
507 *Rhodobacter capsulatus cbb* operons. *J Bacteriol*. 1998;180:4258-69.
508 7. **Falcone DL, Tabita FR**. Expression of endogenous and foreign ribulose 1,5-
509 bisphosphate carboxylase-oxygenase (RubisCO) genes in a RubisCO deletion mutant of
510 *Rhodobacter sphaeroides*. *J Bacteriol*. 1991;173:2099-108.
511 8. **McCully AL, McKinlay JB**. Disrupting Calvin cycle phosphoribulokinase activity in
512 *Rhodopseudomonas palustris* increases the H_2 yield and specific production rate
513 proportionately. *Int J Hydrogen Energy*. 2016;41:4143-9.
514 9. **Gordon GC, McKinlay JB**. Calvin cycle mutants of photoheterotrophic purple nonsulfur
515 bacteria fail to grow due to an electron imbalance rather than toxic metabolite
516 accumulation. *J Bacteriol*. 2014;196:1231-7.
517 10. **McKinlay JB, Harwood CS**. Carbon dioxide fixation as a central redox cofactor recycling
518 mechanism in bacteria. *Proc Natl Acad Sci U S A*. 2010;107:11669-75.
519 11. **Farmer RM, Laguna R, Panescu J, McCoy A, Logsdon B, Zianni M, et al**. Altered
520 residues in key proteins influence the expression and activity of the nitrogenase
521 complex in an adaptive CO_2 fixation-deficient mutant strain of *Rhodobacter sphaeroides*.
522 *Microbiology*. 2014;160:198-208.
523 12. **Öztürk Y, Gökçe A, Peksel B, Gürgan M, Özgür E, Gündüz U, et al**. Hydrogen
524 production properties of *Rhodobacter capsulatus* with genetically modified redox
525 balancing pathways. *Int J Hydrogen Energy*. 2012;37:2014–20.
526 13. **Wang D, Zhang Y, Pohlmann EL, Li J, Roberts GP**. The poor growth of *Rhodospirillum*
527 *rubrum* mutants lacking RubisCO is due to the accumulation of ribulose-1,5-
528 bisphosphate. *J Bacteriol*. 2011;193:3293-303.
529 14. **Gottschalk G**. Bacterial metabolism. 2 ed. New York, NY: Springer-Verlag; 1986.
530 15. **Carlozzi P, Sacchi A**. Biomass production and studies on *Rhodopseudomonas palustris*
531 grown in an outdoor, temperature controlled, underwater tubular photobioreactor. *J*
532 *Biotechnol*. 2001;88:239-49.
533 16. **Hädicke O, Grammel H, Klamt S**. Metabolic network modeling of redox balancing and
534 biohydrogen production in purple nonsulfur bacteria. *BMC Syst Biol*. 2011;5:150.
535 17. **Wang X, Modak HV, Tabita FR**. Photolithoautotrophic growth and control of CO_2
536 fixation in *Rhodobacter sphaeroides* and *Rhodospirillum rubrum* in the absence of
537 ribulose bisphosphate carboxylase-oxygenase. *J Bacteriol*. 1993;175:7109-14.
538 18. **De Meur Q, Deutschbauer A, Koch M, Wattiez R, Leroy B**. Genetic plasticity and
539 ethylmalonyl coenzyme A pathway during acetate assimilation in *Rhodospirillum*
540 *rubrum* S1H under photoheterotrophic conditions. *Appl Environ Microbiol*. 2018;84:
541 e02038-17.

542 19. **Laguna R, Tabita FR, Alber BE**. Acetate-dependent photoheterotrophic growth and the
543 differential requirement for the Calvin-Benson-Bassham reductive pentose phosphate
544 cycle in *Rhodobacter sphaeroides* and *Rhodopseudomonas palustris*. *Arch Microbiol*.
545 2011;193:151-4.
546 20. **Buchanan BB, Evans MC, Arnon DI**. Ferredoxin-dependent carbon assimilation in
547 *Rhodospirillum rubrum*. *Arch Mikrobiol*. 1967;59:32-40.
548 21. **Joshi HM, Tabita FR**. Induction of carbon monoxide dehydrogenase to facilitate redox
549 balancing in a ribulose bisphosphate carboxylase/oxygenase-deficient mutant strain of
550 *Rhodospirillum rubrum. Arch Microbiol*. 2000;173:193-9.
551 22. **Buescher JM, Antoniewicz MR, Boros LG, Burgess SC, Brunengraber H, Clish CB, et**
552 **al**. A roadmap for interpreting ^{13}C metabolite labeling patterns from cells. *Curr Opin*
553 *Biotechnol*. 2015;34:189-201.
554 23. **Galushko AS, Schink B**. Oxidation of acetate through reactions of the citric acid cycle
555 by *Geobacter sulfurreducens* in pure culture and in syntrophic coculture. *Arch Microbiol*.
556 2000;174:314-21.
557 24. **Young JD**. INCA: a computational platform for isotopically non-stationary metabolic
558 flux analysis. *Bioinformatics.* 2014;30:1333-5.
559 25. **Leroy B, De Meur Q, Moulin C, Wegria G, Wattiez R**. New insight into the
560 photoheterotrophic growth of the isocytrate lyase-lacking purple bacterium
561 *Rhodospirillum rubrum* on acetate. Microbiology. 2015;161:1061-72.
562 26. **Perez-Arellano I, Rubio V, Cervera J**. Mapping active site residues in glutamate-5-
563 kinase. The substrate glutamate and the feed-back inhibitor proline bind at overlapping
564 sites. *FEBS Lett*. 2006;580:6247-53.
565 27. **Caspi R, Billington R, Fulcher CA, Keseler IM, Kothari A, Krummenacker M, et al**.
566 The MetaCyc database of metabolic pathways and enzymes. Nucleic Acids Res.
567 2018;46:D633-D9.
568 28. **Leisinger T, Haas D**. N-Acetylglutamate synthase of *Escherichia coli* regulation of
569 synthesis and activity by arginine. *J Biol Chem*. 1975;250:1690-3.
570 29. **Jiang P, Peliska JA, Ninfa AJ**. The regulation of *Escherichia coli* glutamine synthetase
571 revisited: role of 2-ketoglutarate in the regulation of glutamine synthetase
572 adenylylation state. *Biochemistry*. 1998;37:12802-10.
573 30. **Miller RE, Stadtman ER**. Glutamate synthase from *Escherichia coli*. An iron-sulfide
574 flavoprotein. *J Biol Chem*. 1972;247:7407-19.
575 31. **Wang D, Zhang Y, Welch E, Li J, Roberts GP**. Elimination of Rubisco alters the
576 regulation of nitrogenase activity and increases hydrogen production in *Rhodospirillum*
577 *rubrum*. *Int J Hydrogen Energy*. 2010;35:7377-85.
578 32. **Risso C, Van Dien SJ, Orloff A, Lovley DR, Coppi MV**. Elucidation of an alternate
579 isoleucine biosynthesis pathway in *Geobacter sulfurreducens. J Bacteriol*.
580 2008;190:2266-74.
581 33. **Westfall HN, Charon NW, Peterson DE**. Multiple pathways for isoleucine biosynthesis
582 in the spirochete *Leptospira. J Bacteriol*. 1983;154:846-53.
583 34. **Wu B, Zhang B, Feng X, Rubens JR, Huang R, Hicks LM, et al.** Alternative isoleucine
584 synthesis pathway in cyanobacterial species. *Microbiology*. 2010;156:596-602.
585 35. **Eisenstein E, Yu HD, Schwarz FP**. Cooperative binding of the feedback modifiers
586 isoleucine and valine to biosynthetic threonine deaminase from *Escherichia coli*. *J Biol*
587 *Chem*. 1994;269:29423-9.

588 36. **Xu H, Zhang Y, Guo X, Ren S, Staempfli AA, Chiao J, et al**. Isoleucine biosynthesis in
589 *Leptospira interrogans* serotype lai strain 56601 proceeds via a threonine-independent
590 pathway. *J Bacteriol*. 2004;186:5400-9.
591 37. **Rizk ML, Laguna R, Smith KM, Tabita FR, Liao JC**. Redox homeostasis phenotypes in
592 RubisCO-deficient *Rhodobacter sphaeroides* via ensemble modeling. *Biotechnol Prog*.
593 2011;27:15-22.
594 38. **Hiraishi A**. Fumarate reduction systems in members of the family *Rhodospirillaceae*
595 with different quinone types. *Arch Microbiol*. 1988;150:56-60.
596 39. **Beatty JT, Gest H**. Generation of succinyl-coenzyme A in photosynthetic bacteria. *Arch*
597 *Microbiol*. 1981;129:335-40.
598 40. **Ramana VV, Chakravarthy SK, Raj PS, Kumar BV, Shobha E, Ramaprasad EV, et al**.
599 Descriptions of *Rhodopseudomonas parapalustris* sp. nov., *Rhodopseudomonas*
600 *harwoodiae* sp. nov. and *Rhodopseudomonas pseudopalustris* sp. nov., and emended
601 description of *Rhodopseudomonas palustris*. *Int J Syst Evol Microbiol*. 2012;62:1790-8.
602 41. **Hiraishi A, Hoshino Y**. Distribution of rhodoquinone in Rhodosprillaceae and its
603 taxonomic implications. *J Gen Appl Microbiol*. 1984;30:435-48.
604 42. **Ramirez-Ponce MP, Ramirez JM, Gimenez-Gallego G**. Rhodoquinone as a constituent
605 of the dark electron-transfer system of *Rhodospirillum rubrum*. *FEBS Lett*.
606 1980;119:137-40.
607 43. **Larimer FW, Chain P, Hauser L, Lamerdin J, Malfatti S, Do L, et al**. Complete genome
608 sequence of the metabolically versatile photosynthetic bacterium *Rhodopseudomonas*
609 *palustris*. *Nat Biotechnol*. 2004;22:55-61.
610 44. **Lonjers ZT, Dickson EL, Chu TP, Kreutz JE, Neacsu FA, Anders KR, et al**.
611 Identification of a new gene required for the biosynthesis of rhodoquinone in
612 *Rhodospirillum rubrum. J Bacteriol*. 2012;194:965-71.
613 45. **Li F, Hagemeier CH, Seedorf H, Gottschalk G, Thauer RK**. *Re*-citrate synthase from
614 *Clostridium kluyveri* is phylogenetically related to homocitrate synthase and
615 isopropylmalate synthase rather than to *Si*-citrate synthase. *J Bacteriol*. 2007;189:4299-
616 304.
617 46. **Kim M, Le HM, Xie X, Feng X, Tang YJ, Mouttaki H, et al**. Two pathways for glutamate
618 biosynthesis in the syntrophic bacterium *Syntrophus aciditrophicus*. *Appl Environ*
619 *Microbiol*. 2015;81:8434-44.
620 47. **Fitzmaurice WP, Saari LL, Lowery RG, Ludden PW, Roberts GP**. Genes coding for the
621 reversible ADP-ribosylation system of dinitrogenase reductase from *Rhodospirillum*
622 *rubrum. Mol Gen Genet*. 1989;218:340-7.
623 48. **Kim M, Harwood CS**. Regulation of benzoate-CoA ligase in *Rhodopseudomonas*
624 *palustris. FEMS Microbiol Lett*. 1991;83:199-203.
625 49. **Kearns DB, Losick R**. Swarming motility in undomesticated *Bacillus subtilis. Mol*
626 *Microbiol*. 2003;49:581-90.
627 50. **Huang JJ, Heiniger EK, McKinlay JB, Harwood CS**. Production of hydrogen gas from
628 light and the inorganic electron donor thiosulfate by *Rhodopseudomonas palustris. Appl*
629 *Environ Microbiol*. 2010;76:7717-22.
630 51. **McKinlay JB, Zeikus JG, Vieille C**. Insights into *Actinobacillus succinogenes*
631 fermentative metabolism in a chemically defined growth medium. *Appl Environ*
632 *Microbiol*. 2005;71:6651-6.

633 52. **Xia Y, Lu C, Hou N, Xin Y, Liu J, Liu H, et al**. Sulfide production and oxidation by
634 heterotrophic bacteria under aerobic conditions. *ISME J*. 2017;11:2754-66.
635 53. **McKinlay JB, Shachar-Hill Y, Zeikus JG, Vieille C**. Determining *Actinobacillus*
636 *succinogenes* metabolic pathways and fluxes by NMR and GC-MS analyses of ^{13}C-labeled
637 metabolic product isotopomers. *Metab Eng.* 2007;9:177-92.
638 54. **Millard P, Letisse F, Sokol S, Portais JC**. IsoCor: correcting MS data in isotope labeling
639 experiments. *Bioinformatics*. 2012;28:1294-6.
640 55. **Quandt J, Hynes MF**. Versatile suicide vectors which allow direct selection for gene
641 replacement in gram-negative bacteria. *Gene.* 1993;127:15-21.
642
643

644

645 **Table 1. Oxidation states of substrates mentioned in this study relative to biomass.**

Substrate	Formula	Oxidation state[a] 646
carbon dioxide	CO_2	+4 647
formate	CH_2O_2	+2 648
fumarate	$C_4H_4O_4$	+1 649
malate	$C_4H_6O_5$	+1 650
succinate	$C_4H_6O_4$	+0.5 651
acetate	$C_2H_4O_2$	0 652
biomass	$CH_{1.8}N_{0.18}O_{0.38}$	-0.5 653

654

655 [a]Values were determined for each carbon atom as described previously (10, 14) and then
656 averaged by dividing the sum by the number of carbon atoms. Formulas for the acids of organic
657 acids are shown.

658 [b]Biomass composition of *R. palustris* 42OL was used (15).

659 **Figures and legends**

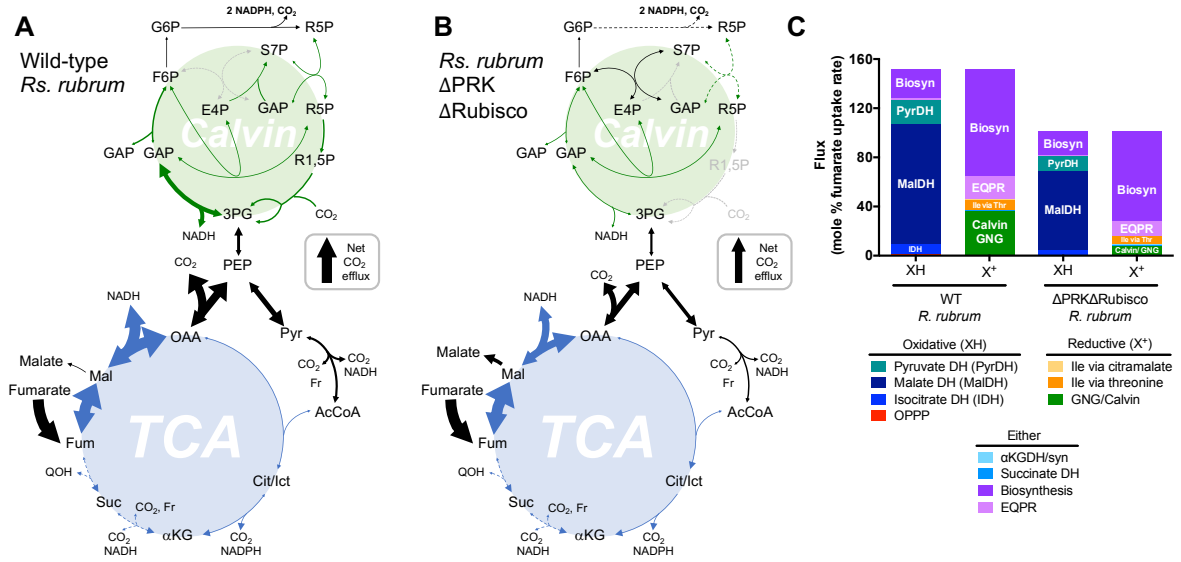

660

661 **Fig. 1. ^{13}C-tracer experiments suggest net reductive TCA flux to αKG in *Rs. rubrum* grown**

662 **on fumarate.** (A, B) Optimal flux solutions for WT *Rs. rubrum* (UR2) (A) and the

663 ΔPRKΔRubisco mutant (UR2557) (B) grown phototrophically on [1,4-^{13}C]fumarate. Flux

664 magnitudes (mol % of the fumarate uptake rate) are indicated by solid arrow thickness. Dashed

665 arrows indicate fluxes with magnitudes less than 1 mol % of the fumarate uptake rate. Net flux

666 direction is indicated by an enlarged arrowhead. (C) Comparison of fluxes through redox

667 reactions. XH columns refer to oxidative pathways that reduce electron carriers, whereas X^+

668 columns refer to reductive pathways that oxidize electron carriers. EQPR is the synthesis of Glu,

669 Gln, Pro, and Arg estimated from the total flux to αKG multiplied by the proportion of αKG used

670 for each amino acid (Table S3) and then by the number of oxidation or reduction steps in each

671 synthesis pathway. DH, dehydrogenase; OPPP, oxidative pentose phosphate pathway;

672 aKGDH/syn, αKG DH/synthase; GNG/Calvin, glyceraldehyde-3-phosphate DH in either

673 gluconeogenesis (GNG) or the Calvin cycle (Calvin). (A-C) Absolute flux values were 1.73 ±

674 0.09 and 0.66 ± 0.16 mmol fumarate/g DCW/h ± SD for the WT strain and the ΔPRKΔRubisco

675 mutant, respectively. All flux values are in Table S4.

676

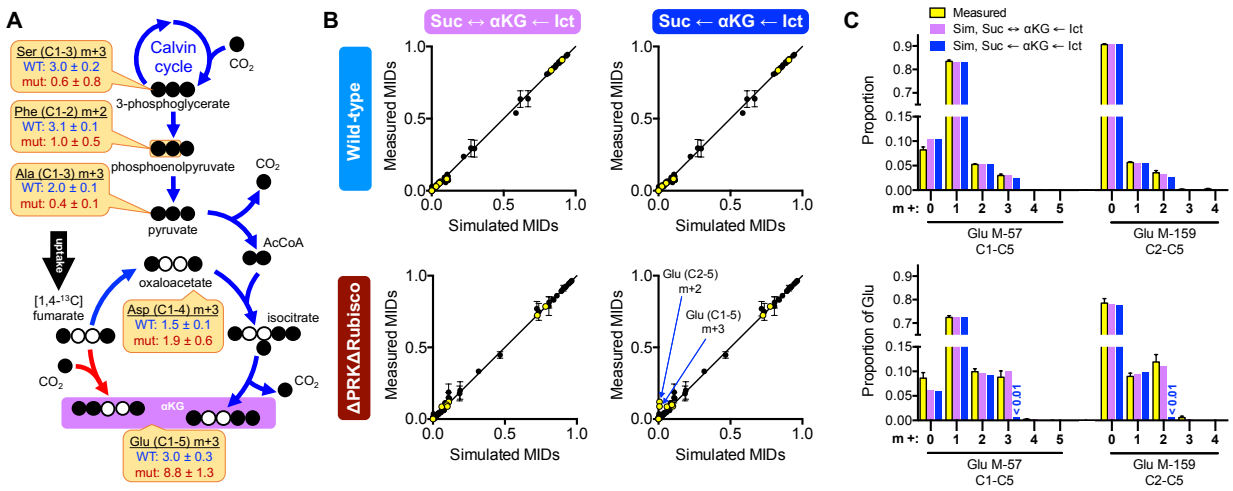

677

678 **Fig. 2. m+3 Glu is a signature of reductive flux from [1,4-^{13}C]fumarate to αKG in the *Rs.***

679 ***rubrum* ΔPRKΔRubisco mutant.** (A) m+3 Glu can be generated by both the Calvin cycle and

680 reductive flux to αKG (red). However, the proportion of m+3 Asp is insufficient to explain the

681 proportion of m+3 Glu by oxidative flux to αKG alone (blue). Yellow boxes show proportions

682 for the indicated mass isotopomer ± SD. Decarboxylation reactions are the source of $^{13}CO_2$ for

683 carboxylation reactions. White, ^{12}C; black, ^{13}C. (B, C) Top, WT *Rs. rubrum* (UR2); bottom, *Rs.*

684 *rubrum* ΔPRKΔRubisco (UR2557). (B) Linear regression of measured vs simulated MIDs from

685 the optimal flux solutions for strains grown with [1,4-^{13}C]fumarate. Simulations used a flux

686 model that either allowed (left) or did not allow (right) for reversible flux between succinate

687 (Suc) and αKG (αKG synthase). Irreversible flux from isocitrate (Ict) to αKG was assumed for

688 all flux models. Yellow, Glu MIDs; black, MIDs for all other examined amino acids. (C)

689 Comparison of measured and simulated (Sim) Glu MIDs from both models used in panel B.

690 Error bars, SD; n = 4.

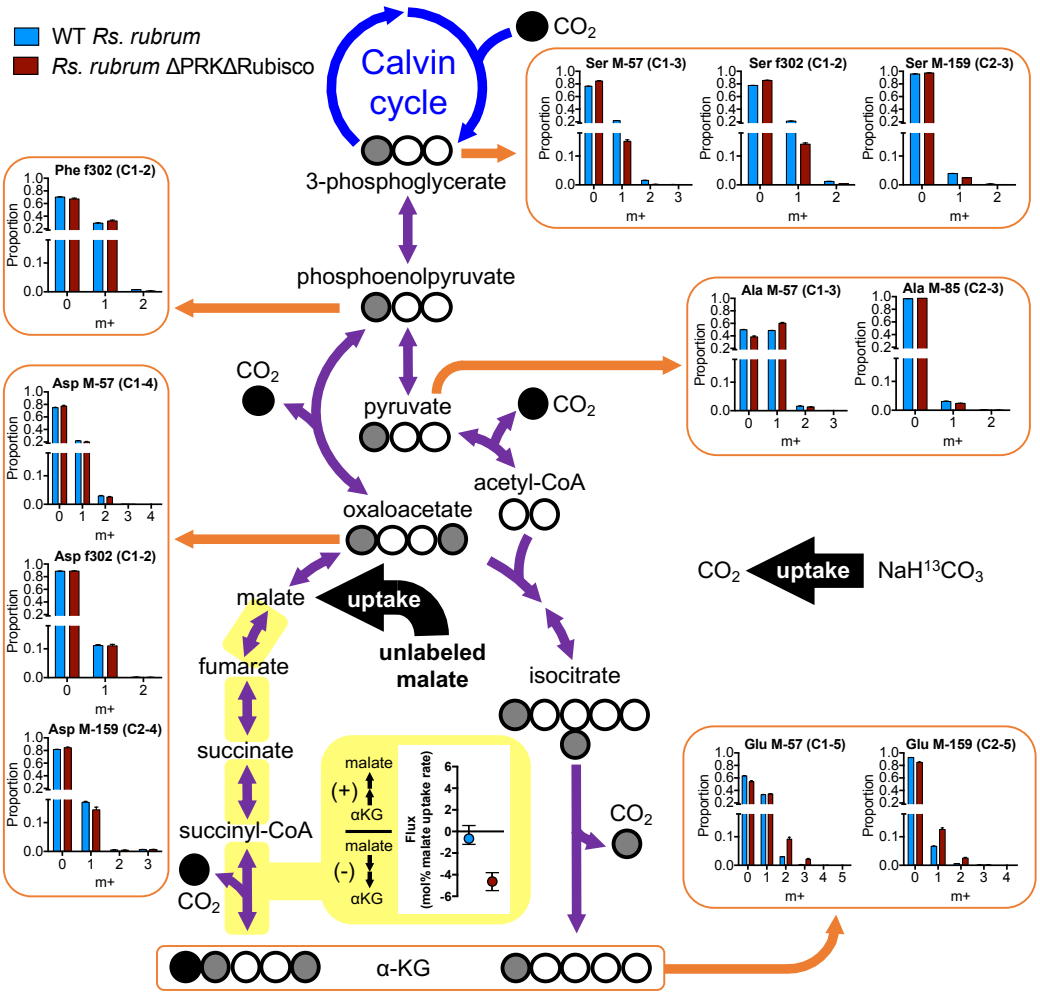

Fig. 3. Flux estimates from experiments with unlabeled malate and NaH^{13}CO$_3$ suggest reductive net flux from malate to αKG in WT *Rs. rubrum* (UR2) and the ΔPRKΔRubisco mutant (UR2557). Only reductive flux to αKG can explain the high proportions of m+1, m+2, and m+3 Glu, all derived from αKG, relative to the corresponding MIDs of aspartate, derived from oxaloacetate. White, ^{12}C; black, ^{13}C; gray, partial labeling. Yellow inset: net flux value estimates between succinate and αKG (αKG synthase) with non-symmetrical upper and lower bounds determined by parameter continuation. Similar net flux values were obtained from malate to αKG (Table S4).

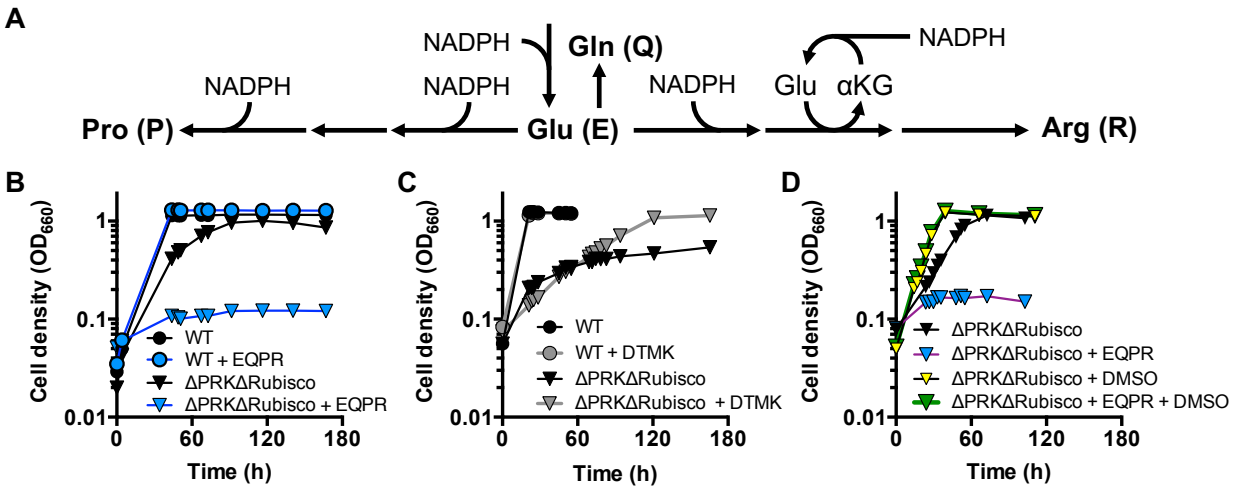

Fig. 4. αKG-derived amino acids repress phototrophic growth of the *Rs. rubrum* ΔPRKΔRubisco mutant on malate. (A) Simplified pathway illustrating the redox reactions involved in the synthesis of the four amino acids synthesized from αKG. (B-D) Growth curves for WT *Rs. rubrum* and the ΔPRKΔRubisco mutant grown with a mixture of either glutamate, glutamine, proline, and arginine (EQPR) (B), with or without DMSO (D), or aspartate, threonine, methione, and lysine (DTMK) (C).

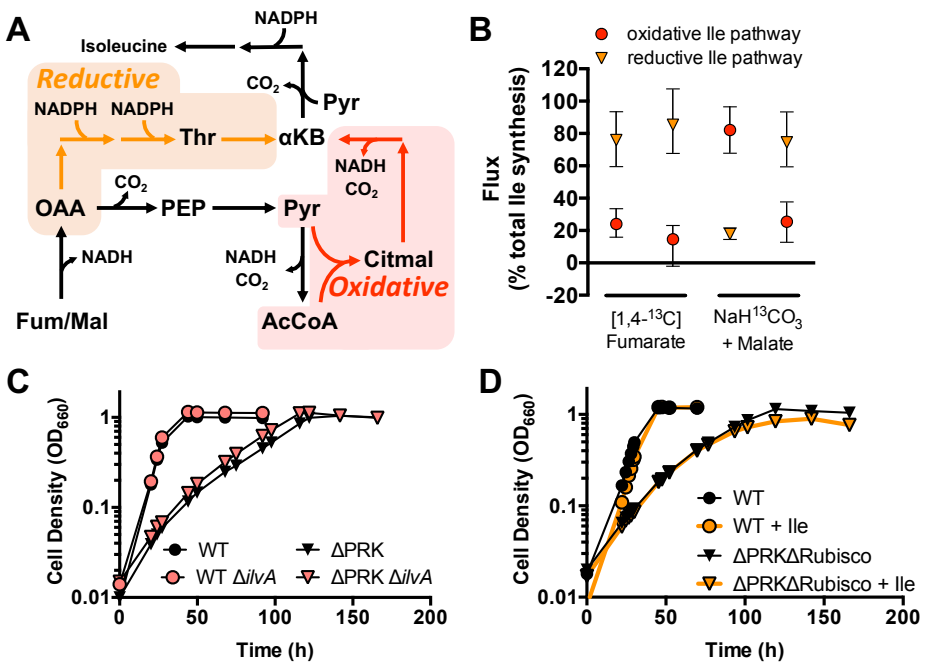

Fig. 5. A non-essential reductive isoleucine synthesis pathway is favored in *Rs. rubrum* in the absence of the Calvin cycle. (A) *Rs. rubrum* has two pathways for isoleucine synthesis. The canonical threonine-dependent pathway (orange) is reductive, whereas the alternative citramalate-dependent pathway (red) is oxidative during growth on malate or fumarate. αKB, α-ketobutyrate. (B) Estimated fluxes as a percent of total isoleucine synthesis for the oxidative citramalate-dependent pathway and the reductive threonine-dependent pathway for the WT (UR2) and ΔPRKΔRubisco (UR2557) strains during growth on either [1,4-^{13}C]fumarate or malate with $NaH^{13}CO_3$. All flux values are in Table S4. (C) Growth trends of WT and ΔPRK (UR2565) strains with or without deletion of *ilvA*, which encodes threonine deaminase in the reductive threonine-dependent pathway. (D) Growth trends of WT and ΔPRKΔRubisco strains with or without added isoleucine in the medium.

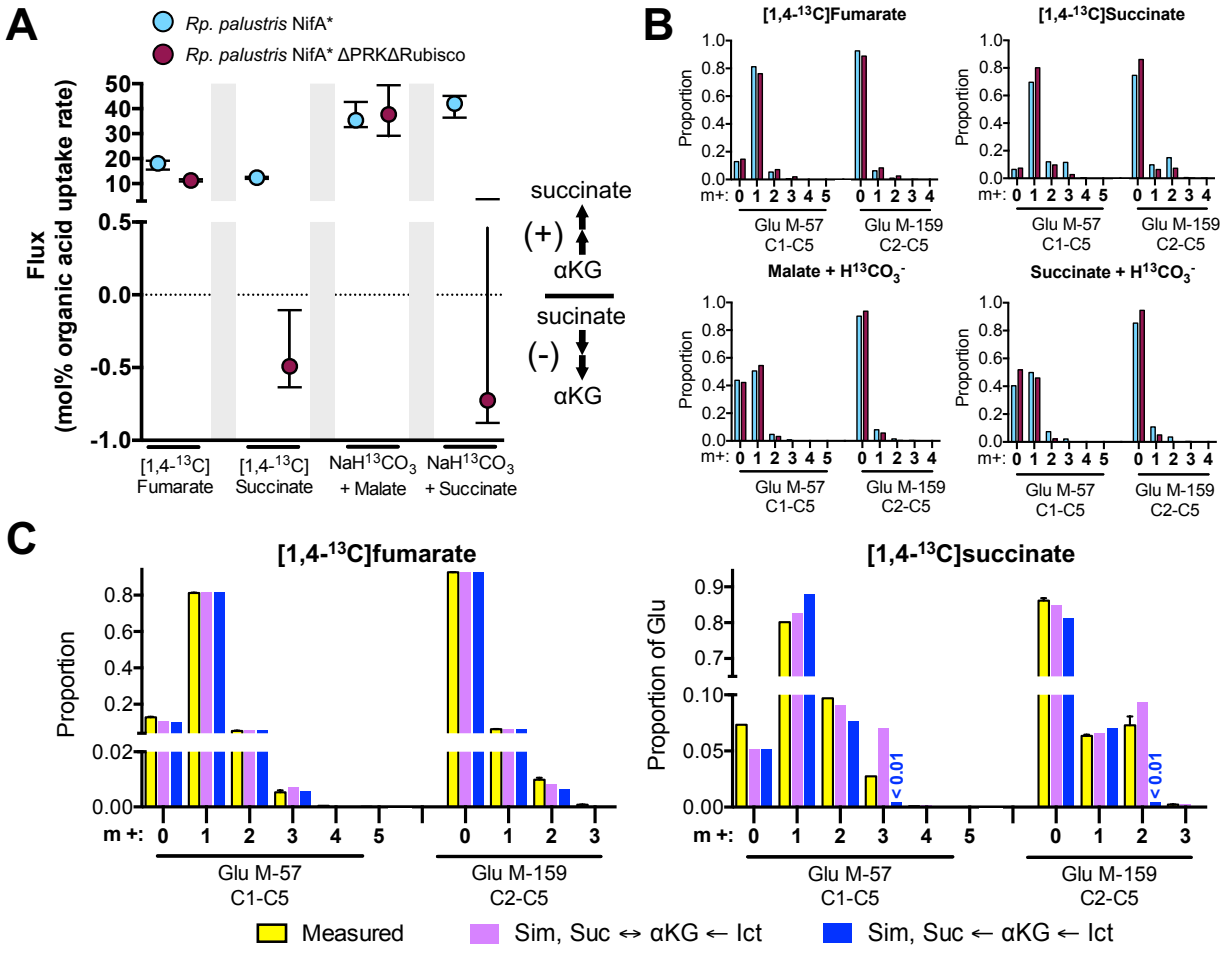

Fig. 6. ^{13}C-labeling experiments suggest that *Rp. palustris* is capable of reductive αKG synthase activity but not fumarate reductase activity. (A, B) Net αKG synthase flux values (A) and Glu MIDs (B) from optimal flux solutions for *Rp. palustris* NifA* (CGA676) and *Rp. palustris* NifA* ΔPRKΔRubisco (CGA4011) grown phototrophically on various labeled substrates. (A) Flux values are mole % of either the fumarate, malate, or succinate uptake rate. Gray bars serve to separate experimental results. All flux values are in Table S4. (B) NifA* Glu MIDs were reported previously (3, 10). (C) Comparison of measured and simulated (Sim) Glu MIDs from models for *Rp. palustris* NifA* ΔPRKΔRubisco. Simulations either allowed or did not allow for reversible flux between succinate and αKG (αKG synthase). Error bars, SD; n = 3.

730 **Supplementary figures and legends**

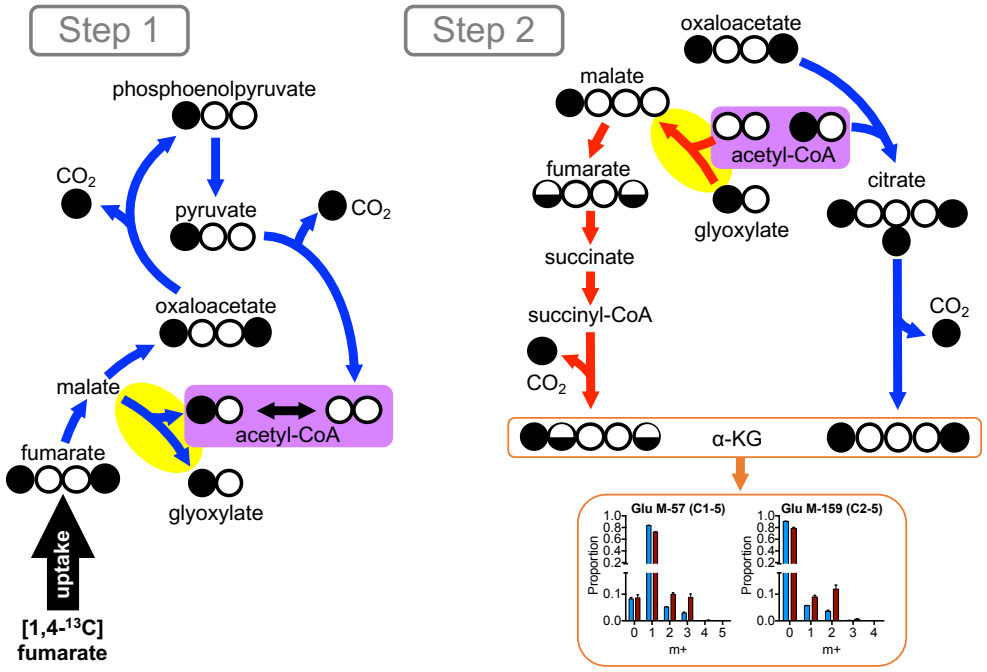

731

732 **Fig. S1. Exchange flux through malate synthase (highlighted yellow) can contribute to the**

733 **generation of m+2 Glu in *Rs. rubrum* during growth on [1,4-^{13}C]fumarate.** Step 1. Reverse

734 malate synthase activity generates single-labeled acetyl-CoA while pyruvate dehydrogenase

735 generates unlabeled acetyl-CoA. Step 2. Forward malate synthase activity combines unlabeled

736 acetyl-CoA with single-labeled glyoxylate to form single-labeled malate. Single-labeled malate

737 can be reduced to double-labeled αKG, serving as a precursor for m+2 Glu. Meanwhile, citrate

738 synthase combines double-labeled oxaloacetate and single-labeled acetyl-CoA to generate triple-

739 labeled citrate. Subsequent oxidative decarboxylation leads to double-labeled αKG, serving as

740 another source of m+2 Glu. This latter oxidative route can theoretically still explain the

741 observation of m+2 Glu, but not m+3 Glu, in models that do not allow for reductive flux to αKG

742 (Fig. 2 and 6). White circles, ^{12}C; black circles, ^{13}C; half-filled circles, either ^{12}C or ^{13}C due to

743 scrambling from the symmetry of fumarate and succinate.

744

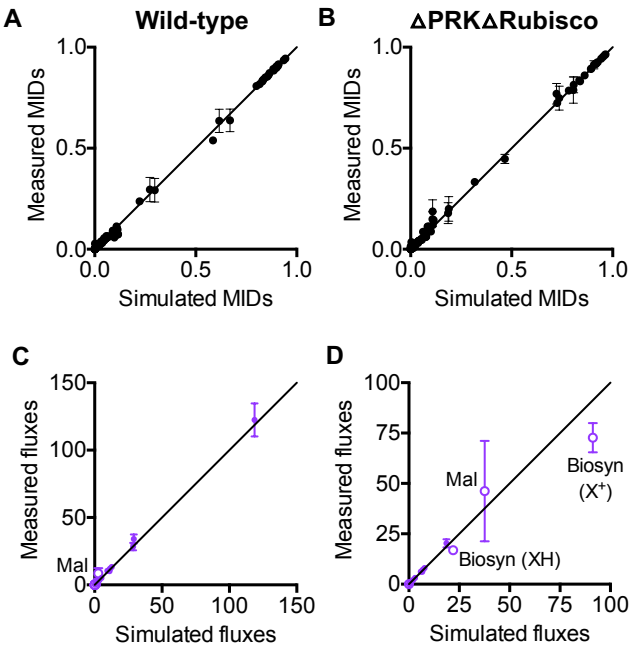

745

746 **Fig. S2. Measured and simulated MIDs and fluxes are similar except for malate excretion**

747 **and biosynthetic redox reactions for *Rs. rubrum*.** Comparison of measured and simulated

748 MIDs (A, B) or flux values (C, D) from optimal flux solutions for WT *Rs. rubrum* (A, C) or the

749 ΔPRKΔRubisco mutant (B, D) grown with [1,4-^{13}C]fumarate. (C, D) Values are mole % of the

750 fumarate uptake rate. Error bars, SD; n = 4 for MIDs and malate excretion. Biosynthetic fluxes

751 were assumed to have an SD of 10% of the mean.

752

753 **Fig. S3. *Rs. rubrum* cultures test negative for sulfide**

754 **production using lead acetate strips.** Strips darken when

755 exposed to sulfide. An aerobic culture of *Bacillus subtilis*

756 3610 grown in LB medium was used as a positive control for

757 sulfide production (52). Similar trends were observed for two

758 other biological replicates.

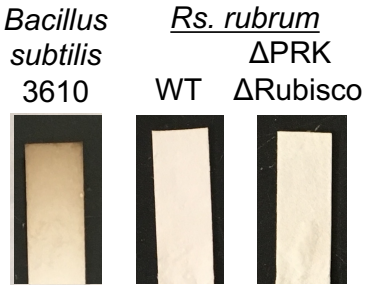

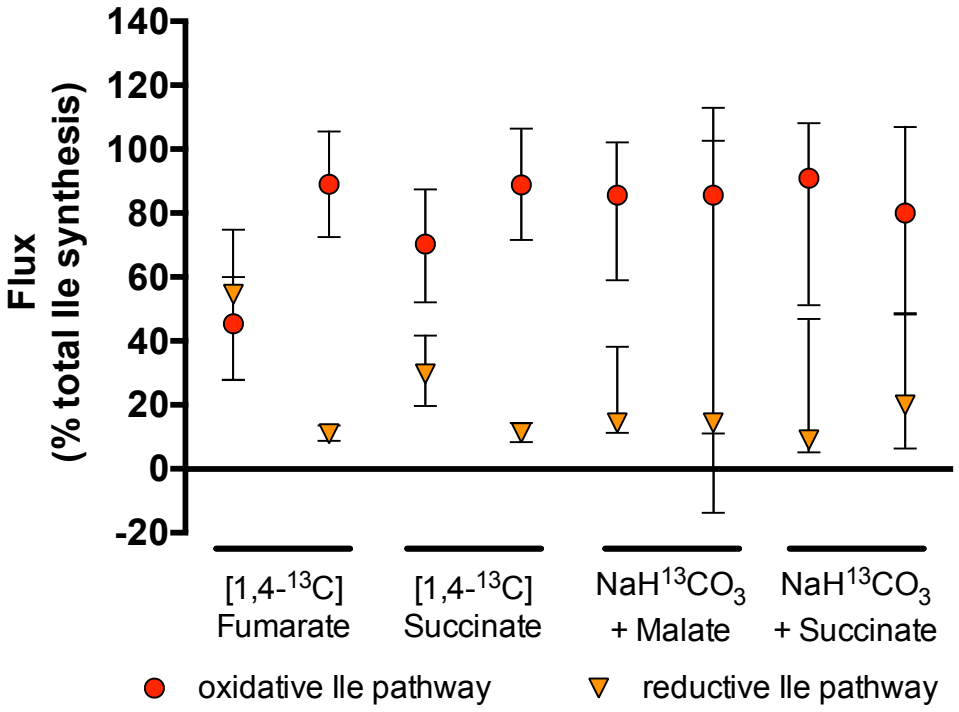

759

760 **Fig. S4. *Rp. palustris* does not adjust fluxes through the reductive and oxidative isoleucine**

761 **synthesis pathways in response to the absence of the Calvin cycle.** Estimated fluxes as a

762 percent of total isoleucine synthesis for the oxidative citramalate-dependent pathway and the

763 reductive threonine-dependent pathway in *Rp. palustris* NifA* (CGA676) and the NifA*

764 ΔPRKΔRubisco strain (CGA4011) during growth on the carbon sources indicated. All flux

765 values are in Table S4.